Local Environment of Yttrium in Y-Doped Barium Cerate Compounds

Alessandro Longo,*,† Francesco Giannici,‡ Antonella Balerna,§ Carmela Ingrao,‡ Francesca Deganello,† and Antonino Martorana‡

Istituto per lo Studio dei Materiali Nanostrutturati, Consiglio Nazionale delle Ricerche, via Ugo La Malfa, 153, I-90146 Palermo, Italy, Dipartimento di Chimica Inorganica e Analitica "Stanislao Cannizzaro", Università di Palermo, viale delle Scienze, I-90128 Palermo, Italy, and Laboratori Nazionali di Frascati, Istituto Nazionale di Fisica Nucleare, via Enrico Fermi 44, I-00044, Frascati, Italy

Received June 29, 2006. Revised Manuscript Received September 4, 2006

The local structure of yttrium in Y-doped $BaCeO_3$ compounds was studied using X-ray absorption spectroscopy (XAS) at the Y K-edge. Data analysis shows that the local environment of Y^{3+} changes, resulting in a distorted octahedron. The structural distortion found does not depend on the dopant amount at the investigated compositions, but on the level of hydration, as clearly demonstrated by the distortion increase in the $BaCe_{0.9}Y_{0.1}O_{3-\delta}$ sample after the treatment in O_2/H_2O. In situ measurements performed in O_2/H_2O flux, which show that the distortion is retained at 753 K, are also reported. The observed significative structural changes seem to point out a preferential insertion of the hydroxyls around the dopant in the Y-doped $BaCeO_3$ compounds.

1. Introduction

Ceramic oxides with the general formula ABO_3 and perovskite-type structure have received considerable attention for the fabrication of high-temperature (600−1000 °C) solid-state protonic conductors, with potential applications in the field of fuel cells and ceramic membrane technology. In this class of materials, $BaCeO_3$-based compounds present the highest protonic conductivity, but an improvement of the chemical stability and proton conductivity is required to implement these materials for the construction of effective electrochemical devices.[1−4] Actually, experimental and theoretical investigations are being performed on barium cerate and other perovskites, to achieve a deeper knowledge of the existing materials and to tailor a new generation of proton conducting ceramics.[5−11]

Introduction of protons in the solid oxide network is achieved by doping the B octahedral site with lower valence cations and with the incorporation of hydroxyls in the so-obtained oxygen-deficient solid according to the reaction:

$$H_2O + O_O^x + V_O^{\bullet\bullet} = 2OH_O^{\bullet} \quad (1)$$

Proton conduction in ceramic oxides involves hopping from a reticular oxygen to an adjacent one. Therefore, the local structure is a key feature of these materials, and in fact it was investigated in many theoretical studies, also in relation with the mechanism of proton diffusion. As concerns in particular $BaCeO_3$, the energetics of proton and dopant incorporation was investigated by Glöckner et al.[12] and by Wu et al.,[5] while Kreuer and Münch et al. found by quantum molecular dynamics simulations that the reduction of the local symmetry due to the presence of the dopant produces an increase in the activation energy of proton hopping.[13,14] Many studies concern other proton conducting perovskites: for instance, molecular dynamics simulation on Sc-doped strontium titanate demonstrated different electronic environments for Ti and Sc and allowed one to investigate possible migration paths for the proton;[15] density functional theory (DFT) calculations were applied to study the geometry of the local environment and the effect of proton insertion in zirconates $AZrO_3$ (A = Ca, Sr, Ba) doped with trivalent species;[16,17] the proton-transfer mechanism in $CaZrO_3$ was investigated by DFT, allowing one to demonstrate a different

* Corresponding author. E-mail: alex@pa.ismn.cnr.it.
† Consiglio Nazionale delle Ricerche.
‡ Università di Palermo.
§ Istituto Nazionale di Fisica Nucleare.

(1) Iwahara, H.; Asakura, Y.; Katahira, K.; Tanaka, M. *Solid State Ionics* **2004**, *168*, 299−310.
(2) Kreuer, K. D. *Solid State Ionics* **2000**, *136−137*, 149−160.
(3) Kreuer, K. D. *Annu. Rev. Mater. Res.* **2003**, *33*, 333−359.
(4) Norby, T. *Solid State Ionics* **1999**, *125*, 1−11.
(5) Wu, J.; Davies, R. A.; Islam, M. S.; Haile, S. M. *Chem. Mater.* **2005**, *17*, 846−851.
(6) Mather, G. C.; Islam, M. S. *Chem. Mater.* **2005**, *17*, 1736−1744.
(7) Ruiz-Trejo, E.; De Souza, R. A. *J. Solid State Chem.* **2005**, *178*, 1959−1967.
(8) Shimura, T.; Tanaka, H.; Matsumoto, H.; Yogo, T. *Solid State Ionics* **2005**, *176*, 2945−2950.
(9) Thundathil, M. A.; Jones, C. Y.; Snyder, G. J.; Haile, S. M. *Chem. Mater.* **2005**, *17*, 5146−5154.
(10) Ranran, P.; Yan, W.; Lizhai, Y.; Zongqiang, M. *Solid State Ionics* **2006**, *177*, 389−393.
(11) Karlsson, M.; Matic, A.; Berastegui, P.; Börjesson, L. *Solid State Ionics* **2005**, *176*, 2971−2974.
(12) Glöckner, R.; Islam, M. S.; Norby, T. *Solid State Ionics* **1999**, *122*, 145−156.
(13) Kreuer, K. D. *Solid State Ionics* **1999**, *125*, 285−302.
(14) Münch, W.; Kreuer, K. D.; Seifert, G.; Maier, J. *Solid State Ionics* **2000**, *136−137*, 183−189.
(15) Shimojo, F.; Hoshino, K.; Okazaki, H. *J. Phys: Condens. Matter* **1998**, *10*, 285−294.
(16) Shi, C.; Yoshino, M.; Morinaga, M. *Solid State Ionics* **2005**, *176*, 1091−1096.
(17) Yoshino, M.; Liu, Y.; Tatsumi, K.; Tanaka, I.; Morinaga, M.; Adachi, H. *Solid State Ionics* **2003**, *162−163*, 127−133.

10.1021/cm0615018 CCC: $33.50
Published on Web 11/07/2006

behavior of oxygens located in inequivalent crystallographic sites.[18]

It is rather surprising that, in comparison with the several theoretical studies, only a very limited number of papers are dedicated to the study of the local structure of proton conducting perovskites by experimental methods. In particular, just a few XAFS (X-ray absorption fine structure) studies concern Yb:$SrCeO_3$,[19] Yb:$SrZrO_3$,[20] lanthanide-doped $CaZrO_3$,[21,22] and Ce-, Nd-, and U-doped calcium titanate;[23] concerning barium cerate, only one partial account exists in the literature about an XAFS experiment on $BaCe_{1-x}Y_xO_{3-\delta}$,[24] while a very recent paper investigates dopant partitioning over Ba and Ce sites in Gd- and Yb-doped barium cerate.[25]

On the side of the crystallographic structure, the structure and phase transitions of barium cerate, neodymium-doped and yttrium-doped barium cerate were investigated by neutron diffraction as a function of dopant amount and of temperature.[26,27] Takeuchi et al. studied the crystal structure of water-bearing and dried Y:$BaCeO_3$ compounds over a wide range of dopant concentrations.[28] Time-of-flight neutron scattering experiments carried out at 4 K allowed Knight to determine the preferential site for proton insertion.[29] The fulfillment of Vegard's law in various trivalent ion-doped cerates was investigated by X-ray diffraction as a function of dopant type and dopant amount by Kruth et al.[30] The cited authors argued that the anomalous behavior of the lattice constants of these compounds could be attributed to BO_6 octahedra local distortion or to defect association and put these structural features in relation with the amount of water uptake.

Effectively, the analysis of diffraction data allows one to determine only the average structure of a crystalline matrix modified by the hosted species; hence, the study of local deviations from an ideal periodicity in the environment of the dopant or in the site of insertion of the proton is a necessary complement of long-range structural investigations on proton conducting ceramics and an important validation tool for theoretical studies on the proton-transfer mechanism. In this paper, we report a detailed analysis of the local environment of yttrium in Y-doped barium cerate compounds. Two very different dopant levels were studied: 10% Y-doping of the cerium site corresponds to the dopant amount used by Knight for the neutron scattering study on the crystallographic structure of Y:$BaCeO_3$,[27] while 2% Y-doping was chosen with the aim of minimizing possible structural effects due to defect interactions. Fully dehydrated and as-prepared samples were analyzed. The 10% Y-doped compound was also measured at 120 K after treatment with H_2O/O_2 and at 753 K in flowing wet oxygen. The latter experiment was carried out with a special cell for in situ treatments, which allows one to measure samples in a controlled environment and also to collect spectra in the range of temperatures from 120 to 773 K in fluorescence and transmission geometry.[31] To our knowledge, this is the first time that an X-ray absorption experiment is performed on a proton conducting ceramic material in operative conditions.

2. Experimental Section

2.1. Materials and Synthesis. The doped barium cerate powders were prepared by citrate-nitrate auto-combustion synthesis. Stoichiometric amounts of Ce(III) nitrate (99.999%), Y(III) nitrate (99.9%), and Ba(II) nitrate (99.999%) shipped by Aldrich were dissolved in distilled water, and afterward citric acid (99.5% Merck) was added to achieve a two-fold citric acid/metal nitrates ratio. Next, ammonium nitrate (99% Merck) was added to regulate the fuel/oxidant ratio (citric acid/nitrate) of the solution to 0.4. The pH of the resulting mixture was adjusted to 6 with NH_3 solution (30 wt %). Water was evaporated at 353 K under constant stirring, until a sticky gel was obtained. The temperature of the bath was then raised gradually to 473 K up to the formation of a black powder. Finally, the powder was directly heated on a hot plate between 523 and 573 K, and self-ignition occurred after a few minutes. The spontaneous combustion lasted for about 10−20 s, resulting in a sponge-like solid, which was then calcined in laboratory air at 1273 K for 5 h. The general stoichiometric formula of the so obtained samples can be written as $BaCe_{1-x}Y_xO_{3-\delta}$, where x is equal to 0.02, 0.1, and δ represents the oxygen deficiency. Because no weight loss occurred during the spontaneous combustion and the formation of a single perovskite phase was observed by X-ray diffraction (XRD), the powder stoichiometry was calculated from the weighted amounts of metal nitrates before they were dissolved in water. High-purity yttrium oxide (99.999%), used as reference material for X-ray absorption experiments, was shipped by Aldrich, and its structure was checked by X-ray diffraction.

2.2. X-ray Diffraction. XRD patterns were recorded in Bragg−Brentano geometry using a PW1710 diffractometer (Philips) with Ni-filtered Cu K_α radiation. The powder patterns were collected using a step size of 0.05° and a counting time of 5 s. The complete Rietveld analysis of XRD powder patterns was performed using GSAS, with Tchebischeff polynomials for the background subtraction and Pearson VII functions for the peak shape.[32]

2.3. X-ray Absorption. X-ray absorption spectra at the Y K-edge (17.038 keV) were recorded at the GILDA-BM8 beamline of the European Synchrotron Radiation Facility (ESRF).[33] The X-ray beam

(18) Islam, M. S.; Davies, R. A.; Gale, J. D. *Chem. Mater.* **2001**, *13*, 2049−2055.
(19) Arita, Y.; Yamasaki, S.; Matsui, T.; Harami, T.; Kobayashi, K. *Solid State Ionics* **1999**, *121*, 225−228.
(20) Kamishima, O.; Ohta, K.; Chiba, Y.; Hattori, T. *J. Phys: Condens. Matter* **2001**, *13*, 2455−2466.
(21) Davies, R. A.; Islam, M. S.; Chadwick, A. V.; Rush, G. E. *Solid State Ionics* **2000**, *130*, 115−122.
(22) Islam, M. S.; Davies, R. A.; Fisher, C. A. J.; Chadwick, A. V. *Solid State Ionics* **2001**, *145*, 333−338.
(23) Hanajiri, Y.; Matsui, T.; Arita, Y.; Nagasaki, T.; Shigematsu, H.; Harami, T. *Solid State Ionics* **1998**, *108*, 343−348.
(24) Matsui, T.; Tokunaga, T.; Nagasaki, T.; Arita, Y.; Shigematsu, H.; Harami, T.; Ohno, H.; Kobayashi, K. *J. Nucl. Mater.* **1997**, *248*, 435−438.
(25) Wu, J.; Webb, S. M.; Brennan, S.; Haile, S. M. *J. Appl. Phys.* **2005**, *97*, 054101−1.
(26) Knight, K. S.; Bonanos, N. *Solid State Ionics* **1995**, *77*, 189−194.
(27) Knight, K. S. *Solid State Ionics* **2001**, *145*, 275−294.
(28) Takeuchi, K.; Loong, C.-K.; Richardson, J. W., Jr.; Guan, J.; Dorris, S. E.; Balachandran, U. *Solid State Ionics* **2000**, *138*, 63−77.
(29) Knight, K. S. *Solid State Ionics* **2000**, *127*, 43−48.
(30) Kruth, A.; Mather, G. C.; Jurado, J. R.; Irvine, J. T. S. *Solid State Ionics* **2005**, *176*, 703−712.
(31) Longo, A.; Balerna, A.; d'Acapito, F.; D'Anca, F.; Giannici, F.; Liotta, L. F.; Pantaleo, G.; Martorana, A. *J. Synchrotron Rad.* **2005**, *12*, 499−505.
(32) Larson, A.; Von Dreele, R. B. *Report LAUR* **1988**, 86−748.
(33) d'Acapito, F.; Colonna, S.; Pascarelli, S.; Antonioli, G.; Balerna, A.; Bazzini, A.; Boscherini, F.; Campolungo, F.; Chini, G.; Dalba, G.; Davoli, I.; Fornasini, P.; Graziola, R.; Licheri, G.; Meneghini, C.; Rocca, F.; Sangiorgio, L.; Sciarra, V.; Tullio, V.; Mobilio, S. *ESRF Newslett.* **1998**, *30*, 42−44.

Table 1. XAFS Fit Results for Yttrium-Doped Barium Cerate with Different Dopant and Water Content[a]

sample	2% fresh	2% dry	10% fresh	10% dry	10% wet	10% wet (753 K)
N_{O1}	4.0 ± 0.5	4.0 ± 0.5	4.2 ± 0.5	4.0 ± 0.5	4.1 ± 0.5	4.1 ± 0.5
R_{O1}	2.23 ± 0.02	2.23 ± 0.02	2.24 ± 0.01	2.25 ± 0.01	2.24 ± 0.01	2.25 ± 0.01
σ_{O1}^2	36 ± 9	25 ± 6	45 ± 11	34 ± 9	46 ± 11	87 ± 22
N_{O2}	2.0 ± 0.5	2.0 ± 0.5	1.9 ± 0.5	2.0 ± 0.5	2.0 ± 0.5	2.0 ± 0.5
R_{O2}	2.33 ± 0.02	2.31 ± 0.02	2.32 ± 0.02	2.30 ± 0.02	2.35 ± 0.02	2.35 ± 0.02
σ_{O2}^2	39 ± 10	40 ± 10	40 ± 10	39 ± 10	41 ± 10	68 ± 16
N_{Ba}	8	8	8	8	8	
R_{Ba}	3.75 ± 0.02	3.76 ± 0.03	3.78 ± 0.02	3.77 ± 0.01	3.79 ± 0.02	
σ_{Ba}^2	132 ± 8	118 ± 8	149 ± 8	109 ± 8	145 ± 8	
N_{M1}	6	6	6	6	6	
θ	159 ± 4	158 ± 5	159 ± 2	159 ± 2	160 ± 2	
$\sigma\theta$	4 ± 0.5	4 ± 0.6	13 ± 0.3	6 ± 0.2	24 ± 0.3	
N_{M2}	12	12	12	12	12	
R_{M2}	6.23 ± 0.03	6.22 ± 0.03	6.24 ± 0.01	6.23 ± 0.01	6.26 ± 0.01	
σ_{M2}^2	120 ± 20	73 ± 20	120 ± 10	109 ± 10	160 ± 10	

[a] Distances are reported in angstroms, σ^2 in 10^{-4} Å^2, angles in degrees, and σ_θ in square degrees. Y−M1 distances and σ^2 are calculated from θ and σ_θ.

was monochromatized by a Si (311) double-crystal fixed exit and sagittal focusing monochromator; a couple of grazing incidence Pd coated mirrors were used for higher-order harmonics rejection. Absorption spectra were taken in transmission mode on the reference yttrium oxide (Y_2O_3), and on the 10% yttrium-doped barium cerate samples. Two krypton-filled ionization chambers were used to detect the incident, I_0, and, respectively, the transmitted, I_t, intensity, thus allowing one to determine the absorption signal as $\mu(E) = \ln(I_0/I_t)$. In transmission mode, to achieve a very good S/N ratio (10^4), the monochromator was operated without focusing. For the dilute samples (2% of yttrium), the fluorescence mode was necessary, and in this case the dynamical sagittal focusing of the monochromator was used, allowing one to achieve a very high photon flux (approximately 10^{11} ph/s) at the sample position. The absorption signal in fluorescence mode is defined as $\mu(E) = I_f/I_0$. The yttrium fluorescence intensity I_f was detected using a 13-elements Ge multidetector. The samples for XAS experiments were ground in a mortar, mixed with a suitable amount of boron nitride, and pressed to form self-supporting pellets. Both 10% and 2% Y-doped samples were measured at liquid nitrogen temperature to reduce the effects of thermal disorder. For each composition, at least two scans were collected. After the measurements on the as-prepared samples, labeled as "fresh" in the forthcoming figures and Table 1, pure dry oxygen was flushed at 1073 K to ensure complete deprotonation.[28] Samples subjected to this treatment are denominated "dry". Liquid nitrogen measurements were performed also on dry samples. To study the local environment of yttrium at high temperature in protonated compounds, the in situ XAFS pattern of the 10% Y-doped sample was recorded in water-saturated oxygen flux at 753 K and, as a low-temperature reference, also at 120 K not removing the sample from the special cell.[31] In these conditions, it is likely that the "wet" samples measured at 120 and 753 K are at the maximum hydration level, corresponding to about 85% of filled oxygen vacancies.[34]

To determine the local structure, XAFS spectra can be analyzed using various procedures; in this specific case, the GNXAS package was used.[35,36] Using GNXAS the average local environment of the photoabsorber is described in terms of *n*-body distribution functions. For each geometrical configuration associated with 2, 3, and 4 neighboring atoms, the atomic phase shifts are calculated using the most appropriate exchange and correlation potentials in the muffin tin approximation. The use of complex Hedin−Lundqvist potentials permits a correct inclusion of the effects due to inelastic losses. Each *n*-atoms configuration contributes to one or more *n*-body XAFS signals, known as $\gamma^{(n)}$. These functions are calculated using fast algorithms, which take into account the effects of all possible single and multiple scattering (MS) paths.[37] For each $\gamma^{(n)}$, the interatomic distance, coordination number, angle (if $n > 2$), and Debye−Waller factor related to the effect of thermal disorder are included. The theoretical XAFS signal, $\chi(k)$, is given by the sum of all of the $\gamma^{(n)}$ values:

$$\chi(k) = \sum n\gamma^{(n)} \tag{2}$$

where $k = [(2m_e/h^2)(E - E_0)]^{1/2}$ is the modulus of the photoelectron wave vector, E is the photon energy, E_0 is the energy value corresponding to the maximum derivative of the absorption coefficient at the absorption edge, and m_e is the mass of the electron.

The structural parameters are then obtained using a fitting procedure that optimizes the agreement between a model XAFS signal, $\alpha_{mod}(E)$, and the experimental X-ray absorption signal, $\alpha_{exp}(E)$. $\alpha_{mod}(E)$ is obtained by adding a suitable background model to the structural oscillations $\chi_{mod}(k)$ calculated with eq 1. Therefore, the model absorption as a function of the photon energy E is given by:

$$\alpha_{mod}(E) = J\sigma_0(E)[1 + S_0^2\chi_{mod}(E - E_0) + \alpha_{mod}(E) + \alpha_{background}(E) + \alpha_{excitation}(E)] \tag{3}$$

The S_0^2 is a constant reduction factor, which accounts for a uniform reduction of the amplitude of the XAFS signal, associated with many-body effects. $\sigma_0(E)$ is an arctangent steplike function that reproduces the atomic cross section of the atom of interest. The $\alpha_{background}(E)$ is a smooth polynomial spline function accounting for the pre- and postedge contribution of all absorption channels. The last term $\alpha_{excitation}(E)$ normally takes into account the possible presence of multielectron excitations in the absorber atom that add one or more edges to the above-reported equation. All of the parameters in $\alpha_{mod}(E)$, and in particular the edge jump J, the superposition integral S_0^2, and the structural parameters of $\chi_{mod}(k)$, are optimized simultaneously by the MINUIT package.[38] The nonlinear multiparametric fit allows one to carry out a detailed error analysis, so achieving a good estimate of the confidence interval on the final results. The statistical errors on the fitting parameters

(34) Kreuer, K. D.; Münch, W.; Ise, M.; He, T.; Fuchs, A.; Traub, U.; Maier, J. *Ber. Bunsen-Ges. Phys. Chem.* **1997**, *101*, 1344−1350.
(35) Filipponi, A.; Di Cicco, A. *Phys. Rev. A* **1995**, *52*, 1072−1078.
(36) Filipponi, A.; Di Cicco, A. *Phys. Rev. B* **1995**, *52*, 15135−15149.
(37) Filipponi, A. *J. Phys.: Condens. Matter* **1991**, *3*, 6489−6507.
(38) James, F. *MINUIT Function Minimization and Error Analysis, CERN Program Library Long Writeup*, 1994; D506.

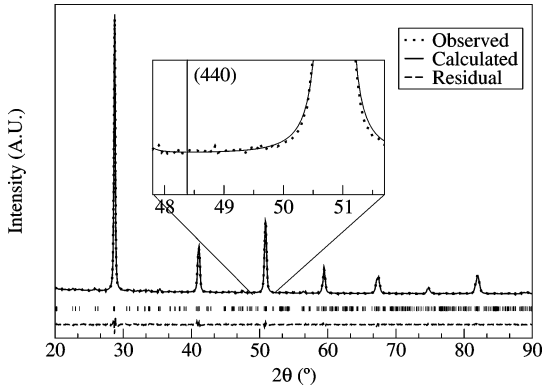

Figure 1. XRD pattern (· · ·) and best fit (−) of fresh $BaCe_{0.9}Y_{0.1}O_{3-\delta}$. The inset shows the absence of the Y_2O_3 phase because its second most intense peak should be, as well known, at 48.5°.

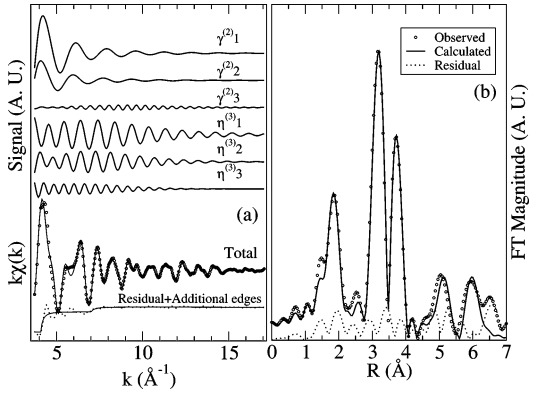

Figure 2. *k*-Weighted *n*-body signals used in the fitting of Y_2O_3. The multielectron excitation term is added to the residual.

are evaluated according to the size of ellipses, which enclose, in the parameter space, χ^2 values with a confidence of 95%.[39]

3. Results and Discussion

Because phase homogeneity is crucial to ensure the reliability of the structural information achievable from XAS data, the fulfillment of this requirement was controlled for fresh and dry samples. The space group used is always *Pmcn* (SG #62), confirming the results of Takeuchi et al. for an yttrium doping amount ≤10%.[28] The Rietveld refinements demonstrate that the samples are homogeneous, as can be seen in Figure 1, relative to the fresh 10% Y-doped sample. The presence of a single crystalline phase is shown by the tickmarks showing the positions of the Y:$BaCeO_3$ lines and by the inset reporting an enlargement of the angular range corresponding to the second most intense yttrium oxide peak that should be at $2\theta = 48.5°$.

The spectrum of yttrium oxide and the spectra of the Y-doped samples were analyzed using a k^3 weighting. As described in the previous section, the calculation of the overall atomic background is carried out at once with the refinement of the structural parameters. The latter are determined on the basis of the crystal structure of yttrium oxide, Mn_2O_3-like (SG #206, Ia3-), which has two different yttrium sites: site 1 with a regular octahedral environment of oxygens and site 2, corresponding to a distorted octahedral coordination. The fitting of the XAFS signal of Y_2O_3 is reported in Figure 2. The component signals are shown: the three $\gamma^{(2)}$, 2-body terms correspond, respectively, to two Y−O bond lengths (first coordination shell) and to a Y−Y direct distance; the 3-body terms $\eta^{(3)}$ are relative to Y−O−Y configurations. In such configurations, the arrangement of the photoabsorber can be depicted as a triangle in which the smaller sides are first shell Y−O distances; by minimization with respect to the angle between the shorter sides, the Y−Y bond length is automatically determined. The residual of the fitting (dotted line) is added to the multielectron excitations term $\alpha_{excitation}$ (see eq 3), corresponding to the transitions [1s3d$_{3/2}$] and [1s4s] at energies $\Delta E = 47 \pm 5$ eV and $\Delta E = 175.5 \pm 10$ eV above the *K* threshold, respectively.[40−42] It is evident the relevance of $\alpha_{excitation}$ with respect to the XAFS signal. Because the coordination numbers of yttria are known, the fitting of the bulk compound allowed also to calibrate the correct value of the S_0^2 parameter. The fitting of an XAFS spectrum of an Y-doped barium cerate is reported in Figure 3.

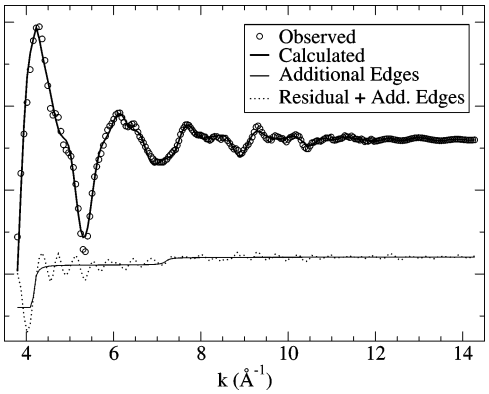

Figure 3. XAFS fitting of the dry $BaCe_{0.9}Y_{0.1}O_{3-\delta}$ sample carried out using the same multielectron edges of Y_2O_3 reference sample.

In the cited neutron scattering study, Knight established that at room temperature undoped $BaCeO_3$ is orthorhombic with space group *Pmcn* and unit cell constants $a = 8.77$ Å, $b = 6.236$ Å, $c = 6.216$ Å.[27] The perovskite-like structure is constituted by a three-dimensional array of very regular and tilted corner-sharing CeO_6 octahedra. For the 10% Y-doping, the same space group was determined, suggesting that no significant perturbation involving long-range order is introduced by the hosted trivalent cation.[27] A fragment of the structure of Y-doped barium cerate, as determined by neutron scattering,[27] is drawn in Figure 4. The *n*-body configuration relevant for the XAFS analysis of the Y environment is also shown, labeling one of the cations in the B-octahedral site as "Y" to indicate the X-ray absorber.

Referring to the Knight's structure, the first shell around yttrium is constituted of six oxygen atoms spanning the range of distances between 2.23 and 2.25 Å; the second shell is formed by eight Ba^{2+} cations at about 3.8 Å. The third shell involves six M1 atoms (M1 = Ce, Y) in corner sharing octahedra at about 4.39 Å, and the fourth shell is constituted

(39) Filipponi, A. *J. Phys.: Condens. Matter* **1995**, *7*, 9343−9356.

(40) Diaz-Moreno, S.; Munoz-Pàez, A.; Chaboy, J. *J. Phys. Chem. A* **2000**, *104*, 1278−1286.

(41) Chaboy, J.; Tyson, T. A. *Phys. Rev. B* **1994**, *49*, 5869−5875.

(42) Chaboy, J.; Marcelli, A.; Tyson, T. A. *Phys. Rev. B* **1994**, *49*, 11652−11661.

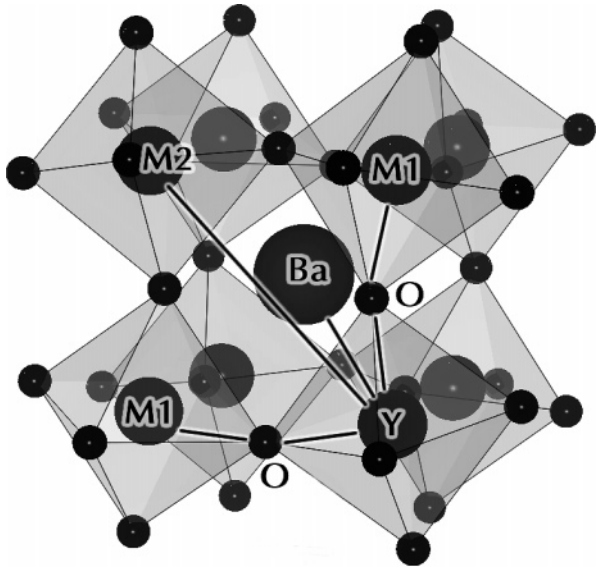

Figure 4. Fragment of the crystal structure of Y:$BaCeO_3$ determined by neutron scattering. The *n*-body paths used in the XAFS analysis are indicated.

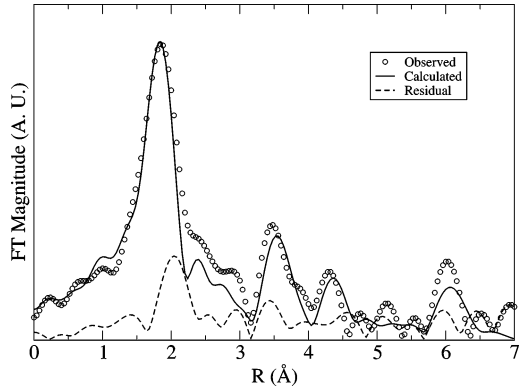

Figure 5. Fourier transform of XAFS data and model relative to dry $BaCe_{0.98}Y_{0.02}O_{3-\delta}$. The model FT corresponds to a regular octahedral oxygen shell around yttrium.

by 12 M2 (M2 = Ce, Y) atoms in the second-neighboring octahedra at about 6.23 Å.

In our analysis, the precision of the XAFS estimate of absorber−backscatterer distance is about 0.02 Å, and therefore the refinement of the Y environment starting from the crystallographic structure was performed using only one Y−O and one Y−Ba 2-body signal, respectively, for the first and second coordination shells, an average contribution relative to the different Y−O−M1 triangles for the third shell, and one 2-body signal corresponding to the fourth shell, Y−M2, direct distance.

At a first glance, the radial distribution function (RDF) around yttrium, obtained by optimizing the parameters relative to the above-described *n*-body signals, gives a general satisfactory agreement with the experimental data (see Figure 5, showing the RDF, not corrected for phase-shift, relative to the dry $BaCe_{0.98}Y_{0.02}O_{3-\delta}$ sample). However, a closer look at Figure 5 shows that this model is not completely able to describe the first coordination shell of yttrium, as evidenced by the peak at 2.32 Å in the difference pattern or residual. This result suggests that the Y closest neighborhood could be a distorted octahedron of oxygens, needing at least one further Y−O distance to be suitably simulated, or, alternatively, that an yttria-like local environment occurs, characterized therefore by two different octahedral environments. To resolve this ambiguity, the XANES (X-ray absorption near-edge structure) spectra of Y-doped barium cerate samples were analyzed.

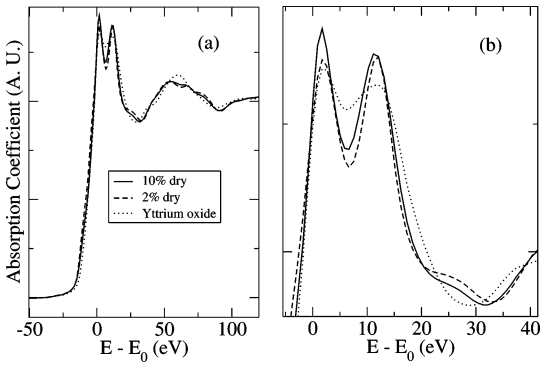

Figure 6. (a) Normalized XANES spectra of the dry samples and of the Y_2O_3 standard. (b) Enlargement of the edge region.

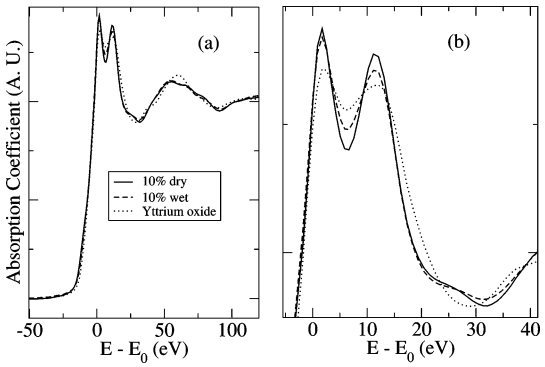

Figure 7. (a) Normalized XANES spectra of the 10%-doped wet and dry samples and of the Y_2O_3 standard. (b) Enlargement of the edge region.

By comparing in Figure 6 the XANES spectra of the reference yttrium oxide and of the two dry Y-doped barium cerate samples, it is evident that the XANES features of these two samples are quite similar with respect to the width and position, while the features in the Y_2O_3 spectrum are definitely broader. Malvestuto et al. have shown that information on the different Y sites can be obtained by XANES simulation with full multiple scattering calculation and proved that the presence of two inequivalent yttrium sites in Y_2O_3 produces an overall noticeable broadening of the XANES features. The same broadened features were also detected in very thin Y_2O_3 films, proving that the yttria-like environment keeps its fingerprints also in the near-edge spectra of very small clusters.[43] Therefore, it can be argued that the yttrium environment in the two Y-doped $BaCeO_3$ samples is clearly different from the Y_2O_3 one, whose absence is also confirmed by the XRD data (see Figure 1). On the other hand, the water uptake changes the XANES features of the 10% Y-doped barium cerate sample, as shown in Figure 7, meaning that the sites of incorporation of the hydroxyl ions should be mainly located in the first coordination shell of Y^{3+}.

(43) Malvestuto, M.; Carboni, R.; Boscherini, F.; d'Acapito, F.; Spiga, S.; Fanciulli, M.; Dimoulas, A.; Vellianitis, G.; Mavrou, G. *Phys. Rev. B* **2005**, *71*, 75318-1−75318-8.

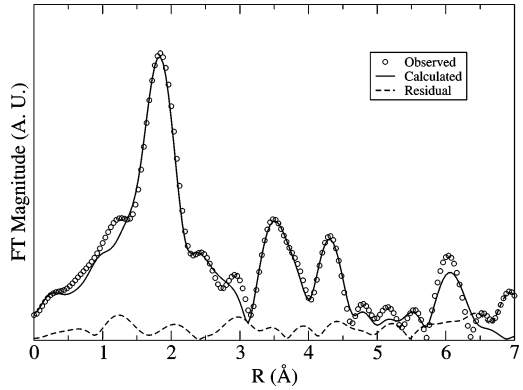

Figure 8. Fourier transform of XAFS data and model of the dry $BaCe_{0.98}Y_{0.02}O_{3-\delta}$ assuming a distorted octahedral yttrium environment.

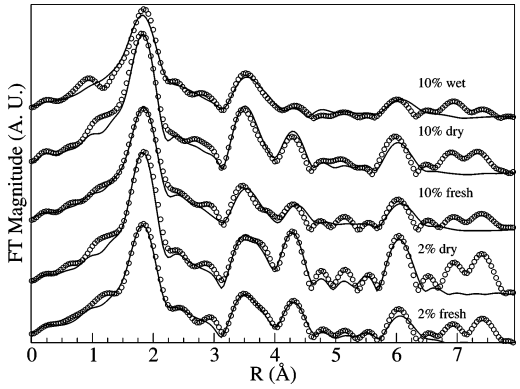

Figure 9. *k*-Weighted Fourier transform of all samples measured at low temperature and best fittings.

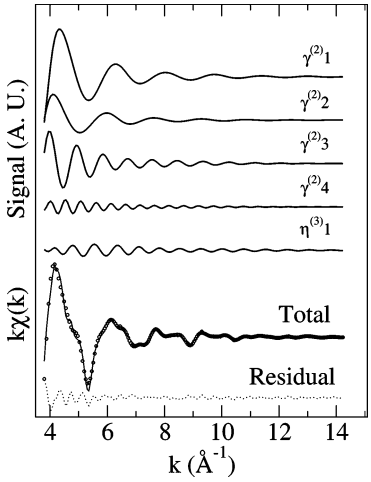

Figure 10. *n*-Body signals used in the fitting of dry $BaCe_{0.98}Y_{0.02}O_{3-\delta}$.

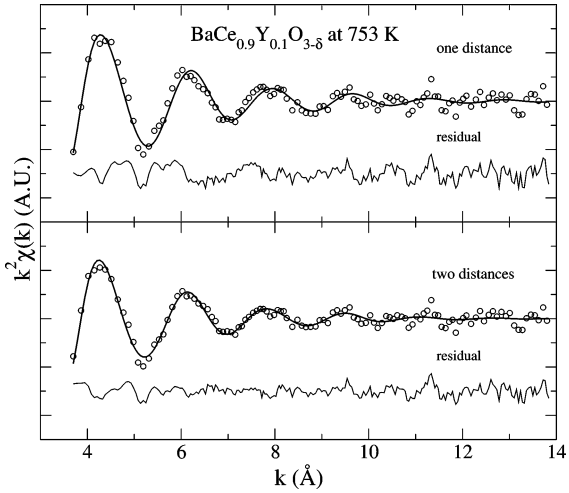

Figure 11. In situ XAFS of $BaCe_{0.9}Y_{0.1}O_{3-\delta}$ measured at 753 K in O_2/H_2O atmosphere (○) together with best fit (line). Upper panel shows the best fit with a regular YO_6 octahedron. Lower panel shows the best fit with a distorted octahedron including two Y−O distances.

A possible partitioning of yttrium between the two different cationic sites A and B is excluded by simulations of the XAFS signal and is in agreement with the theoretical forecast of Wu et al.[5] Moreover, this demonstrates that Y^{3+} partially substitutes Ce^{4+} and allows water incorporation according to eq 1.

From all of these considerations, it comes out that yttrium is located in a single site, characterized by a distorted octahedral distribution of oxygens.

The results of the XAFS analysis carried out on the basis of the assumption of two different Y−O distances are reported in Table 1. As can be seen from the inspection of Table 1, the XAFS analysis of the Y-doped barium cerate samples was carried out taking into account four 2-body signals (Y−O1, Y−O2, Y−Ba, and Y−M2) and one 3-body Y−O−M1 component, taking into account the average of the Y−O−M1 contributions between corner-sharing octahedra, as can be seen in Figure 4. The latter term allows one to get the Y−M1 average distance by optimization of the Y−$\hat{O}$−M1 θ angle. The coordination numbers varied within the error around the crystallographic values 8, 6, and 12, respectively, for the Y−Ba, Y−M1, and Y−M2 coordination shells, and therefore were kept fixed in the final fittings. The coordination numbers of the Y−O1 and Y−O2 shells were allowed to vary, but, as can be seen from the results reported in Table 1, the optimized values were always close to 4 and 2 and do not vary with hydration. On the other hand, the indetermination on the coordination number intrinsically given by XAFS spectroscopy does not allow one to discriminate the vacancy−dopant association present in Y-doped barium cerate. Figure 8 shows that the introduction in the model of a second Y−O distance produces a huge improvement of the fitting, as compared to the one reported in Figure 5. It is not excluded that the introduction of further distances in the model could improve the agreement with the data. However, taking into account the goodness of the fitting reported in Figure 8, it is likely that a finer discrimination falls within the EXAFS sensitivity. Figure 9 reports the Fourier transform magnitudes for the different samples. The *n*-body signals used in the fitting procedure are reported in Figure 10.

Despite the high temperature and the damping of the XAFS signal, due to the high values of Debye−Waller factors, the fine structures of the spectrum taken at 753 K in H_2O-saturated O_2 flux are clearly visible, as shown in Figure 11. As a first attempt, a fitting of the data was performed using a 2-body configuration related to the first shell Y−O distance, in which all oxygen atoms are at the same distance. As shown in Figure 11 (upper panel), using a single distance, a low frequency is detectable in the difference pattern, while when fitting the data with two Y−O distances (lower panel) a better agreement is achieved.

By inspection of Table 1, some aspects can be pointed out:

(i) The first coordination shell of yttrium is characterized by two different Y−O1 and Y−O2 distances, likely corresponding, in comparison to the nearly regular CeO_6 octahedron in barium cerate-based compounds, to an expanded and distorted YO_6 octahedron. Moreover, the difference between the Y−O1 and the Y−O2 distances is larger in the 10% Y-doped wet sample, with respect to the dry one. As pointed out by Kreuer, this distortion could produce a significant reduction of proton mobility.[13]

(ii) The overall XAFS results relative to yttrium−oxygen distance and Debye−Waller factors confirm the evidence coming from XANES that the dopant first coordination shell is modified by hydration and therefore that the oxygen vacancies in the dry samples are preferentially located in the neighborhood of yttrium. This conclusion corroborates with experimental data the theoretical forecast of Glöckner, Islam, and Norby, who calculated a strong $Y^{3+}-V_O^{\bullet\bullet}$ binding energy.[12]

(iii) The Y−O distances in wet O_2 flux at 753 K are the same as the one found at liquid nitrogen temperature, demonstrating that high-temperature treatments in humid ambient do not modify the first coordination shell of yttrium. This result shows that the local structure of the Y is retained also in conditions similar to operative as concerns temperature and chemical environment.

(iv) With respect to the higher coordination shells, it can be observed that the Debye−Waller factors of the Y−Ba and Y−M2 coordination shells clearly increase with the water content. The visual comparison of the radial distribution functions reported in Figure 9 confirms this evidence, especially concerning the third shell-peak in the 4−4.5 Å range, simultaneously affected by the Y−O Debye−Waller factors and by the variance σ_θ on the θ angle. This result can depend on the hydroxyls incorporation in the immediate neighborhood of the dopant. The scientific debate about the localization of protonic defects near the dopant sites is open, and the size of the dopant is, in this respect, an important parameter to be taken into account. The results of X-ray absorption on Y-doped barium cerate point to dopant−defect association; however, it is worth remarking that experimental work carried out with TGA concludes that defects are on the contrary delocalized over the whole oxide matrix.[34]

XAFS spectroscopy cannot determine whether protons in ceramic oxides are completely free to diffuse in the matrix, or can be trapped by a strong hydroxyl−dopant interaction, as was demonstrated by theoretical means for $CaZrO_3$ doped with trivalent species[18] and by quasi-elastic neutron scattering in Yb-doped strontium cerate at temperatures as high as 1073 K.[44] However, this study demonstrates that yttrium doping produces a remarkable local distortion in the $BaCeO_3$ matrix both in the dry and in the protonated samples, thus giving rise to possible limitations in proton mobility.[13,14,18]

4. Conclusions

XAFS experiments on $BaCe_{1-x}Y_xO_{3-\delta}$ ($x = 0.02, 0.1$) compounds have been performed on dry and water bearing samples to investigate the local environment of yttrium. The main results can be summarized as follows: the local environment of yttrium is a distorted octahedron of oxygens, characterized by at least two Y−O distances; a significative structural modification in the neighborhood of yttrium takes place under hydration, pointing out a preferential insertion of the hydroxyls in the immediate environment of the dopant; the Debye−Waller factors are larger in protonated samples, and it is likely that also static disorder is effective when water is introduced in the host matrix structure; in situ XAFS experiments performed in O_2/H_2O atmosphere on the 10% Y-doped samples show that the distortion in the YO_6 octahedra observed at liquid nitrogen temperature is retained also at 753 K.

Theoretical approaches investigating the vibrational dynamics of the oxygen sublattice in perovskite-type proton conducting oxides have demonstrated that for each hopping event the oxygen−oxygen distance shortens to assist the proton transfer from one oxygen to the next. Experimental data about local structure could be a useful reference for theoretical calculations to develop a reliable diffusion mechanism for proton conduction and to tailor new generation high-temperature proton conductors.

Acknowledgment. We acknowledge partial financial support from Ministero dell'Università e della Ricerca Scientifica e Tecnologica, Consiglio Nazionale delle Ricerche, and Fondo Integrativo Speciale per la Ricerca (FISR). Fabio D'Anca is acknowledged for technical support during the in situ treatments. VICS-II program has been used to create Figure 4.

CM0615018

(44) Hempelmann, R.; Karmonik, C.; Matzke, T.; Cappadonia, M.; Stimming, U.; Springer, T.; Adams, M. A. *Solid State Ionics* **1995**, *77*, 152−156.